Journal of Mathematical Chemistry Vol. 31, No. 2, February 2002 (© 2002)

Bifurcation phenomena for an oxidation reaction in a continuously stirred tank reactor I. Adiabatic operation

M.I. Nelson and H.S. Sidhu

School of Mathematics and Statistics, University College, University of New South Wales, Australian Defence Force Academy, Canberra 2600, Australia

Received 15 February 2001; revised 2 November 2001

We investigate the steady-state multiplicity exhibited by the reaction of a fuel/air mixture in a continuously stirred tank reactor. The chemical mechanism used is a modification of a scheme due to Sal'nikov. We consider four cases; corresponding to the choice of fuel fraction, inflow temperature, inflow pressure, or precursor decay rate as the primary bifurcation parameter. From the perspective of fire-retardancy, the case when the fuel fraction is varied is the most important. In this case the steady-state diagrams provide a basis for a systematic investigation into the effectiveness of gas-phase active fire retardants.

KEY WORDS: fire-retardants, flammability limits, singularity theory, thermokinetic models

1. Introduction

The continuously-stirred tank reactor (CSTR) is one of the standard types of reactor used in industry. The reactants flow continuously at a known volumetric flow-rate into the reactor and, in order to maintain a constant reaction volume, there is a matching volumetric outflow from the reactor. As a result, chemical species spend only a finite time in the reactor. The CSTR is efficiently stirred so that there are neither any concentration gradients nor a temperature gradient. The bifurcation behaviour of such reactors have been widely investigated in the context of chemical engineering [1]. Particular attention has been paid to models using a first-order nonisothermal irreversible reaction (FONI models).

Traditionally, gas-phase combustion processes were studied in batch reactors. In the early to mid 1970s groups in Leeds and Naples realised that the CSTR offers a much better experimental arrangement [2–6]. In a CSTR true stationary states can be realised and oscillatory behaviour sustained indefinitely. The use of CSTRs was responsible for the advancement in understanding of the mechanism for hydrocarbon oxidation in the 1970s and 1980s and they are now commonly used to study combustion reactions. The absence of spatial gradients permit a stress on the physical chemistry of the problem, without the added complications of fluid flow, and presents an opportunity to validate

detailed kinetic mechanisms through the analysis of the rich variety of phenomena accompanying low temperature oxidation (multiplicity, birhythmicity, cool flames, oscillatory ignition, two-stage and multi-stage ignition, complex ignition, steady ignition etc). There are a number of review articles containing good expository sections on the use of the CSTR in gas-phase combustion studies [7–10].

Here, we investigate the dynamics of a simple gaseous oxidation reaction in a CSTR. Our chemical model is a modified version of a scheme originally proposed by Sal'nikov to explain the phenomena of cool flames [11,12]. Sal'nikov's scheme consists of a two-state decay of a precursor through an intermediate to a final product. Our modification is to introduce an additional chemical species, making the second stage an oxidation reaction. We investigate how the steady-state multiplicity of our model depends upon the choice of primary bifurcation parameter. Three cases are considered when the distinguished parameter is experimentally controllable. These correspond to the choice of either the proportion of precursor to oxygen flowing into the reactor, the inflow temperature, or the inflow pressure as the primary bifurcation parameter. In a fourth case, the effect of changing the decay rate of the precursor species is investigated.

In this paper, we consider the simplifying case when the reactor operates adiabatically, i.e., there is no heat loss between the sides of the reactor and the reaction mixture. The main reason for this assumption is the resulting simplification of the model. However Russo and Bequette [13] have shown that increasing the reactor size causes a reduction in the ratio of heat transfer area to reactor volume. Therefore as the reactor size is increased the effective heat transfer coefficient decreases. As a result, adiabatic operation may be approached when scaling up laboratory sized reactors for industrial operation. Furthermore, combustion in a CSTR can be viewed as an zero-dimensional model for a premixed flame. The assumption of no heat loss therefore equates to a study of an adiabatic flame. It is believed that the treatment of peak premixed flame temperatures as adiabatic is a reasonable approximation [14]. The adiabatic CSTR is, therefore, of independent interest.

In section 1.1 we review work examining the Sal'nikov scheme in well-stirred systems. The appropriate mathematical tool for studying multiplicity in open chemical systems is singularity theory. Section 1.2 contains an overview of this subject.

1.1. The Sal'nikov thermokinetic oscillator

The simplest nonisothermal model generating oscillatory behaviour is due to Sal'nikov [11,12]. Sal'nikov's aim was to explain the occurrence of cool flames observed in the oxidation of hydrocarbons. It is now accepted that the correct description of this phenomenon is the unified chain-thermal theory developed by Gray and Yang [15,16]. Sal'nikov's model retains interest because it provides an archetypal example of nonisothermal chemical oscillations that completely satisfies chemical principles whilst being simple enough to be understood easily and to be analysed deeply. Moreover, as described in section 1.1.4 it has been realised experimentally, thus showing that chemical complexity involving chain branching is not a prerequisite for the existence of thermokinetic oscillations.

Sal'nikov's scheme consists of an exothermic reaction proceeding by two consecutive first-order reactions. A precursor $\mathcal{F}$ generates a reactive species $\mathcal{B}$ which decomposes through an exothermic reaction to an inert product $\mathcal{C}$. It is assumed that all the heat output is associated with the second reaction. This scheme is represented as

$$\mathcal{F} \overset{k_1(T)}{\rightarrow} \mathcal{B} \quad (Q_1 = 0), \tag{1}$$

$$\mathcal{B} \overset{k_2(T)}{\rightarrow} \mathcal{C} \quad (Q_2 \neq 0), \tag{2}$$

where the temperature dependence of the two reaction rates takes Arrhenius form. We refer to the scenario in which the activation energy of the first reaction is zero, i.e., only the second step is responsive to temperature, as a "single Sal'nikov scheme". When both activation energies are nonzero we call the resulting mechanism a "double Sal'nikov scheme". In investigating the behaviour of Sal'nikov schemes it is usually assumed that the precursor species is in excess so that its depletion can be ignored.

Sal'nikov investigated the dynamics of the single and double schemes using techniques from classical dynamical systems theory. He assumed that the reactions took place in a well-stirred batch reactor and that depletion of the precursor species was negligible. A region in parameter space was established in which the system is in a state of undamped oscillations since the relevant phase portrait consists of an unstable steady state surrounded by a stable limit cycle.

1.1.1. The single Sal'nikov scheme

The single Sal'nikov scheme was examined by Gray and Roberts [17] using the techniques of singularity theory. They interpreted the boundary of the region enclosing cool flames as the locus of Hopf bifurcation points in the pressure-ambient temperature plane. A complete description of all the qualitatively distinct behaviour exhibited by the model was obtained, including two regions of parameter space not previously located. Subsequently they investigated two extensions of this work [18]. Firstly, the limiting asymptotic behaviour was obtained exactly as the dimensionless heat capacity tends to zero. Secondly, the effects of including fuel consumption was studied both numerically and in a second asymptotic-limit as the rate of fuel consumption tends to zero.

Simultaneously with the work of Gray and Roberts, the single Sal'nikov scheme was investigated by a group at the University of Leeds [19–21]. A drawback of this work is the use of a nondimensionalisation scheme popularised by Frank-Kamenetskii. These variables have the disadvantage that a key experimental control parameter, the ambient temperature, appears in more than one dimensionless variable. It is therefore difficult to directly relate the results of bifurcation analysis to experimental data. The disadvantages of using the Frank-Kamenetskii variables are discussed elsewhere [22–24]. The work in Leeds was not as comprehensive as that reported by Gray and Roberts.

Forbes [25] has provided a rigorous proof of the nonexistence of oscillations in certain regions of parameter space. Although the Frank-Kamenetskii variables were

used, the results are of a form whereby their dependence upon the ambient temperature–pressure can be extracted. Moreira and Yuquan [26], also using the Frank-Kamenetskii variables, established conditions under which the single Sal'nikov scheme has an unstable limit cycle inside a stable one. The proof requires rewriting the system in the form of a Liénard equation.

The main success of Sal'nikov's scheme is that it can generate thermokinetic oscillations. It is therefore natural to investigate the effect of periodic forcing. Forbes and Gray [27] considered sinusoidal forcing of the ambient temperature. They showed that such forcing can give rise to chaos, which results from either the Feigenbaum period-doubling route or from the Ruelle–Takens approach through quasiperiodicity. Delgado [28] considered forcing of the temperature derivative. In a rather cursory treatment, it is shown that complex and mixed mode oscillations are possible, chaotic behaviour was not found. Delgado [29] then considered periodic forcing of the temperature derivative in a system in which the reactor volume is proportional to the temperature. Under these assumptions a period-doubling route to chaos was found as the amplitude of the forcing term is decreased. It was subsequently demonstrated that unstable periodic orbits embedded in the strange attractor could be stabilised by a continuous delay time method [30]. Delgado has also investigated a thermal engine driven by the single Sal'nikov oscillator [31]. The heat released by the second reaction is used to move a piston which exchanges work between the system and its environment. The piston is shown to have a three-stage cycle comprising nearly isometric, isobaric, and adiabatic branches.

1.1.2. The double Sal'nikov scheme

A preliminary investigation of this scheme was made by Forbes et al. [32]. The border in parameter space between regions possessing one and three equilibria was identified, as was the location of the Hopf locus. They proved that oscillatory behaviour is only possible within a certain region of the parameter space. The definitive analysis of this system was made by Gray and Forbes [33] who showed that it contains 16 qualitatively different phase portraits. A large number of degenerate bifurcations were identified and located, including a spectacularly degenerate Bogdanov–Takens bifurcation that generates three homoclinic bifurcation curves rather than the usual one. Many of these bifurcations are structurally unstable in the sense that their codimension exceeds the number of unfolding parameters. It was shown that the exotic behaviour only occurs if the activation energy of the first reaction is smaller than that of the second, as conjectured by Sal'nikov.

Sexton and Forbes [34] investigated the use of linear control in eliminating oscillations in batch reactor. They showed that oscillatory behaviour can not always be eliminated using negative feedback. In fact, there are circumstances whereby negative feedback creates a worse situation than no feedback, in these conditions positive feedback is required to eliminate limit cycles. In addition, they exhibited a nonlinear feedback control which guarantees no oscillations.

1.1.3. Numerical methods

Sal'nikov schemes typically generate relaxation oscillations of considerable stiffness and special numerical solution techniques are required to obtain periodic solutions. Forbes [25] described a shooting algorithm which gave results of great accuracy, automatically determined the stability of the solution, and was capable of computing unstable periodic orbits. Herges and Twizell [35] computed solutions using the first-order explicit Euler method and an implicit finite-difference method of the same order. Neither of these latter methods were able to compute unstable limit cycles.

1.1.4. Experimental results

The single Sal'nikov scheme has been realised experimentally in a semibatch reactor [19,36–38]. In this work the thermally-neutral temperature-independent decay of the precursor species was mimicked by the physical process of admitting the reactant into the batch reactor at a controlled constant rate via a calibrated capillary leak. The reactant itself, stored in an external reservoir connected to the capillary, constitutes the precursor species.

The dynamics of the decomposition of di-tert-butyl peroxide [19,37,38] and the hydrogen–chlorine reaction [36] have been investigated. The behaviour in both these systems were shown to be satisfactorily explained by a single Sal'nikov scheme. Under the experimental conditions investigated the rate of decomposition of di-tert-butyl peroxide is first order, the exothermicity of the overall reaction is modified in the presence of oxygen but the rate determining step is not changed. This system is, therefore, analogous to a single Sal'nikov scheme. The chemistry of the hydrogen–chlorine reaction is more complicated, comprising five elementary reactions and five chemical species. By making appropriate approximations it is possible to reduce this to a single Sal'nikov scheme. The hydrogen–chlorine system has been investigated by Sidhu et al. [39] who compared the location in parameter space in which oscillations are predicted to occur using the full chemical scheme against that predicted by the Sal'nikov model.

1.2. Singularity theory with a distinguished parameter

The model studied in this paper reduces to a scalar equation of the form,

$$\mathcal{G}\big(T^*, \lambda, \mathbf{p}\big) = 0, \tag{3}$$

see equation (38) in section 3.3. The scalar equation contains a state variable T^*, a distinguished parameter λ, sometimes called the primary bifurcation parameter, and several secondary bifurcation parameters $\mathbf{p}$. The graph of T^* versus λ for fixed $\mathbf{p}$ is called a *steady-state diagram* or a *response curve*. This graph contains *bifurcation points* at which the number of solutions to the equation $\mathcal{G} = 0$ changes. We call a figure showing how the value of λ at which a particular type of bifurcation occurs varies as one of the secondary parameters is changed an *unfolding diagram*.

The parameter space $\mathbf{p}$ consists of regions with different kinds of steady-state diagrams. The fundamental task in the study of equation (3) is to identify the types of

steady-state diagrams that occur and their location in parameter space. We refer to a figure showing where the different types of steady-state diagrams occur in the parameter space **p** as a *bifurcation diagram*. There is no consistency of notation in the literature. What we call a steady-state diagram has been referred to as a bifurcation diagram by some authors. Similarly what we call an unfolding diagram has also been called a bifurcation diagram.

Singularity theory with a distinguished parameter enables degenerate points (singular points) to be located. At these points the boundaries of some of the various regions coalesce, so that several types of steady-state diagrams exist in a neighbourhood of the singularity. The singular points are characterised by the vanishing of several partial derivatives of $\mathcal{G}$ with respect to T^* and λ. The real strength of singularity theory is that it is able to predict all the steady-state diagrams existing locally to a singular point [40].

However, in practice it is important to determine the global existence of the differing types of steady-state diagrams. This is required because parameter values are unlikely to correspond to those in the vicinity of a singular point. The global picture is constructed by determining the locus of the *cusp*, *isola*, and *double limit point* curves in physical parameter space. This method divides parameter space into different regions, each corresponding to a different steady-state diagram of the problem $\mathcal{G} = 0$. (It is therefore a bifurcation diagram in our notation.)

This methodology is based upon Golubitsky and Schaeffer's result that a qualitative change in a steady-state diagram occurs if and only if the bifurcation parameters cross the boundaries of one of these curves [41]. It was first systematically applied to investigate multiplicity features of open chemically reacting systems by Balakotaiah and Luss [42–45]. It is now a standard approach in studying such problems. An attractive feature of this method is that the location of the boundaries is determined directly in the physical parameter space, whereas in singularity theory proper, the boundaries are defined in terms of the unfolding parameters appearing in the normal form of the singularity; in practice it is very difficult to relate the unfolding parameters to the physical ones.

The *cusp variety* is the set of **p** satisfying the equations

$$\mathcal{G} = \mathcal{G}_{T^*} = \mathcal{G}_{T^*T^*} = 0. \tag{4}$$

(A set of nondegeneracy conditions must also be satisfied. These can be found elsewhere [46].) Typically when the cusp curve is crossed a hysteresis loop appears or disappears in the steady-state diagram as two limit points appear or disappear.

The *isola variety* is the set of **p** satisfying the equations

$$\mathcal{G} = \mathcal{G}_{T^*} = \mathcal{G}_{\lambda} = 0. \tag{5}$$

When the isola variety is crossed two limit points appear or disappear. Two types of behaviour may occur. In the first, the steady-state diagrams separate locally into two isolated curves (transcritical singularity). In the second, an isolated branch of connected solutions appears or disappears (isola singularity).

The *double-limit variety* is the set of **p** satisfying the four equations

$$\mathcal{G}\big(T_1^*, \lambda, \mathbf{p}\big) = \mathcal{G}\big(T_2^*, \lambda, \mathbf{p}\big) = 0, \qquad T_1^* \neq T_2^*, \tag{6}$$

$$\frac{\partial \mathcal{G}}{\partial T^*}\big(T_1^*, \lambda, \mathbf{p}\big) = \frac{\partial \mathcal{G}}{\partial T^*}\big(T_2^*, \lambda, \mathbf{p}\big) = 0. \tag{7}$$

At a double-limit point two limit points, at T_1^* and T_2^*, occur at the same value of the distinguished parameter. As the the double limit point variety is crossed the the relative position of these limit points changes.

A heuristic description of this theory with a focus on applications to chemical systems has been written by Balakotaiah [47].

An alternative method to study steady-state diagrams, with particular relevance for the study of chemical systems, is the parametric representation method developed by Simon et al. [48]. This method can be applied when the singularity function takes the special form

$$\mathcal{G} = f_0(x) + u_1 f_1(x) + u_2 f_2(x), \tag{8}$$

where u_1 and u_2 represent a primary bifurcation parameter and an unfolding parameter, respectively.

2. Description of the model

We model a mixture of fuel and air flowing through a diabatic CSTR. We make the standard hypotheses that the reactor vessel has constant volume, perfect mixing and constant physical parameters. The physics of the reactor are described in section 2.1 and the chemical mechanism in section 2.2. Figure 1 shows a simple representation of a CSTR. In section 2.3 we discuss the operation of CSTRs.

2.1. Model physics

The CSTR is assumed to be contained within a circulating air oven giving uniform heating within the enclosure to a given ambient temperature (T_a). The reactants flow

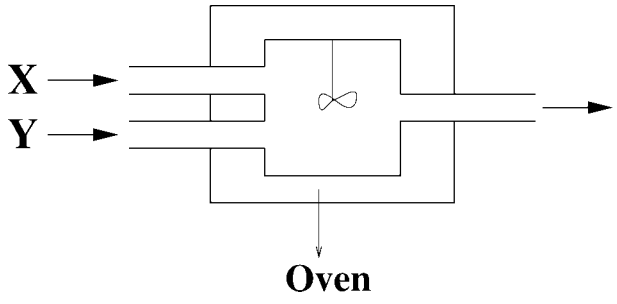

Figure 1. Schematic representation of a CSTR containing a mechanical stirrer with two input chemicals X and Y.

into the reactor through two pipes: the precursor species flows through one pipe and air, considered to be 79% nitrogen and 21% oxygen, through the other. The inflow rates are q_1 and q_2 ($\mathrm{m}^3 \cdot \mathrm{s}^{-1}$), respectively. The outflow rate from the reactor is, therefore, $q_1 + q_2$. The inflow temperatures are assumed to be identical (T_0).

The inflowing air and fuel are at pressures $\mathcal{P}_{\mathrm{air}}$ and $\mathcal{P}_{\mathrm{f}}$, respectively. Assuming ideal gas behaviour the concentrations of the species in the inflow are

$$\mathcal{F}_0 = \frac{\mathcal{P}_{\mathrm{f}}}{RT_0}, \tag{9}$$

$$\mathcal{O}_{2,0} = 0.21\frac{\mathcal{P}_{\mathrm{air}}}{RT_0}, \tag{10}$$

$$\mathcal{N}_{2,0} = 0.79\frac{\mathcal{P}_{\mathrm{air}}}{RT_0}. \tag{11}$$

The total inflow pressure is simply

$$\mathcal{P}_{\mathrm{air}} + \mathcal{P}_{\mathrm{f}} = \mathcal{P}_0. \tag{12}$$

We define the stoichiometry of the inflowing reactants in terms of a fuel fraction variable (α) where

$$\alpha = \frac{\mathcal{P}_{\mathrm{f}}}{\mathcal{P}_0}. \tag{13}$$

Thus, the concentrations of fuel and oxygen flowing into the reactor are proportional to $\alpha\mathcal{P}_0$ and $0.21(1-\alpha)\mathcal{P}_0$, respectively.

Prior to the commencement of the experiment, it is assumed that the entire system is first flushed with the inert nitrogen. Thus the initial concentration of all other chemical species are zero and the initial temperature of the reactor is the corresponding steady-state solution.

For simplicity many parameters, such as the volumetric heat capacity, are assumed to be independent of temperature. In particular, the heat capacity of the contents of the reactor is given by an average value. Thus an equation for the concentration of nitrogen inside the reactor is not required as it does not effect the dynamics of the system.

2.2. *Model chemistry*

We consider an oxidation reaction with the overall representation

$$\mathcal{F} + n\mathcal{O}_2 \rightarrow n\mathcal{C}. \tag{14}$$

The chemical mechanism by which this reaction proceeds is a modified Sal'nikov scheme, section 1.1,

$$\mathcal{F} \overset{k_1}{\rightarrow} n\mathcal{B}, \tag{15}$$

$$\mathcal{B} + \mathcal{O}_2 \overset{k_2(T)}{\rightarrow} \mathcal{C}. \tag{16}$$

The first reaction is assumed to be isothermal, its rate constant does not depend upon the temperature. We have allowed for the possibility that the decay of one mole of the precursor produces more than one mole of fuel ($n > 1$). The second reaction is an exothermic process and its rate constant has an Arrhenius temperature dependence. This is a single Sal'nikov scheme. In previous investigations of such mechanisms it has been assumed that the second reaction is a first order reaction with no dependence upon the concentration of oxygen.

Note that the concentration of the precursor species and oxygen flowing into the reactor are equal when

$$\alpha = 0.21n(1-\alpha), \tag{17}$$

$$\Rightarrow \quad \alpha_{\mathrm{cr}} = \frac{0.21n}{1+0.21n}. \tag{18}$$

Conditions in which $\alpha < \alpha_{\mathrm{cr}}$ ($\alpha > \alpha_{\mathrm{cr}}$) represent fuel-lean (fuel-rich) mixtures, respectively. Where analysis is possible we consider the general case and do not specify the value of n. For numerical purposes we take $n = 1$, for which $\alpha_{\mathrm{cr}} = 0.174$.

2.3. Experimental features

The experimentally controllable parameters are the reactant composition (α), the inflow pressure ($\mathcal{P}_0$), the inflow temperature (T_0), the inflow rates (q_1 and q_2), and the vessel wall temperature (T_{a}). Usually the reactants are preheated to the vessel wall temperature ($T_0 = T_{\mathrm{a}}$) and the flow rates are equal ($q_1 = q_2$). It is convenient to fix the flow rates and the composition, varying the pressure or ambient temperature. One of the principal experimental goals is to establish in the $\mathcal{P}_0$–T_{a} plane, the regions in which the observed phenomena are found, e.g., ignitions and extinctions, cool flames etc. This is effectively the construction of an unfolding diagram. This picture is usually built up from a series of experiments at constant pressure in which the ambient temperature is increased or decreased [8]. Unfolding diagrams of specific systems are discussed in the review articles [8–10].

3. Model equations

3.1. Dimensionalised equations

The system that we study is:

- Concentration of the precursor species

$$V_{\mathrm{g}}\frac{\mathrm{d}\mathcal{F}}{\mathrm{d}t} = q_1\mathcal{F}_0 - (q_1+q_2)\mathcal{F} - V_{\mathrm{g}}A_1\mathcal{F}. \tag{19}$$

- Concentration of fuel

$$V_{\mathrm{g}}\frac{\mathrm{d}\mathcal{B}}{\mathrm{d}t} = -(q_1+q_2)\mathcal{B} + nV_{\mathrm{g}}A_1\mathcal{F} - V_{\mathrm{g}}A_2\exp\left[\frac{-E_2}{RT}\right]\mathcal{B}\mathcal{O}_2. \tag{20}$$

- Concentration of oxygen

$$V_{\mathrm{g}}\frac{\mathrm{d}\mathcal{O}_2}{\mathrm{d}t} = q_2\mathcal{O}_{2,0} - (q_1+q_2)\mathcal{O}_2 - V_{\mathrm{g}}A_2\exp\left[\frac{-E_2}{RT}\right]\mathcal{B}\mathcal{O}_2. \tag{21}$$

- Temperature inside the reactor

$$c_{p_{\mathrm{g}}}\rho_{\mathrm{g}}V_{\mathrm{g}}\frac{\mathrm{d}T}{\mathrm{d}t} = (q_1+q_2)c_{p_{\mathrm{g}}}\rho_{\mathrm{g}}(T_0-T) + Q_2V_{\mathrm{g}}A_2\exp\left[\frac{-E_2}{RT}\right]\mathcal{B}\mathcal{O}_2 - J\chi S(T-T_{\mathrm{a}}). \tag{22}$$

- Concentrations of precursor and oxygen in the inflow

$$\mathcal{F}_0 = \frac{\mathcal{P}_{\mathrm{f}}}{RT_0}, \qquad \mathcal{O}_{2,0} = 0.21\frac{(\mathcal{P}_0-\mathcal{P}_{\mathrm{f}})}{RT_0}. \tag{23}$$

- Initial conditions

$$\mathcal{F}(0) = \mathcal{B}(0) = \mathcal{O}_2(0) = 0, \qquad T(0) = \frac{(q_1+q_2)c_{p_{\mathrm{g}}\rho_{\mathrm{g}}}T_0 + J\chi ST_{\mathrm{a}}}{(q_1+q_2)c_{p_{\mathrm{g}}}\rho_{\mathrm{g}} + J\chi S}. \tag{24}$$

The heat-transfer coefficient has been written as the product $J\chi$ rather than the usual form of χ. We have done this so that we can nondimensionalise time using a Newtonian-cooling time-scale whilst retaining the ability to consider adiabatic operation (adiabatic behaviour corresponds to taking $J = 0$). This avoids the use of different dimensionless schemes for the cases of adiabatic/diabatic behaviour. The remaining terms appearing in equations (19)–(24) are defined in the nomenclature.

3.2. Dimensionless equations

In nondimensionalising equations (19)–(22) we introduce a dimensionless temperature (T^*), dimensionless concentrations ($\mathcal{A}^*, \mathcal{B}^*, \mathcal{O}_2^*$), and a dimensionless time-scale (t^*). These are defined in the nomenclature. Equations (19)–(22) can be written in the dimensionless form:

- Dimensionless precursor concentration

$$\frac{\mathrm{d}\mathcal{F}^*}{\mathrm{d}t^*} = q_1^*\alpha - \left(q_1^*+q_2^*\right)\mathcal{F}^* - A_1^*\mathcal{F}^*. \tag{25}$$

- Dimensionless fuel concentration

$$\frac{\mathrm{d}\mathcal{B}^*}{\mathrm{d}t^*} = -\left(q_1^*+q_2^*\right)\mathcal{B}^* + nA_1^*\mathcal{F}^* - \frac{A_2^*\mathcal{P}^*}{T_0^*}\exp\left[\frac{-E_2^*}{T^*}\right]\mathcal{B}^*\mathcal{O}_2^*. \tag{26}$$

- Dimensionless oxygen concentration

$$\frac{\mathrm{d}\mathcal{O}_2^*}{\mathrm{d}t^*} = 0.21q_2^*(1-\alpha) - \left(q_1^*+q_2^*\right)\mathcal{O}_2^* - \frac{A_2^*\mathcal{P}^*}{T_0^*}\exp\left[\frac{-E_2^*}{T^*}\right]\mathcal{B}^*\mathcal{O}_2^*. \tag{27}$$

- Dimensionless temperature

$$\frac{\mathrm{d}T^*}{\mathrm{d}t^*} = \left(q_1^* + q_2^*\right)\left(T_0^* - T^*\right) + \frac{Q_2^* A_2^* \mathcal{P}^{*^2}}{T_0^{*^2}} \exp\left[\frac{-E_2^*}{T^*}\right]\mathcal{B}^*\mathcal{O}_2^* - J\left(T^* - T_\mathrm{a}^*\right). \tag{28}$$

- Dimensionless initial conditions

$$\mathcal{F}^*(0) = \mathcal{B}^*(0) = \mathcal{O}_2^*(0) = 0, \qquad T^*(0) = \frac{(q_1^* + q_2^*)T_0^* + JT_\mathrm{a}^*}{q_1^* + q_2^* + J}. \tag{29}$$

It is important to note that our aim during the nondimensionalisation process is not to reduce the number of model parameters to their minimal number (which is often the purpose of nondimensionalisation). For example, the dimensionless total inflow pressure ($\mathcal{P}^*$) could be eliminated from equations (25)–(28) by suitably redefining the parameters A_2^* and Q_2^*. However, the total inflow pressure is one of the key experimentally manipulated parameters and should therefore be retained in the governing equations. Our aim in the nondimensionalisation process is to retain experimentally controllable parameters as *distinct* continuation parameters.

3.3. Derivation of the singularity function

Equation (25) shows that the concentration of the precursor species ($\mathcal{F}^*$) does not depend upon any of the other variables in the model ($\mathcal{B}^*, \mathcal{O}_2^*, T^*$). The steady-state, which is reached exponentially in time, is given by

$$\mathcal{F}^* = \frac{q_1^*\alpha}{q_1^* + q_2^* + A_1^*}. \tag{30}$$

In the absence of decay ($A_1^* = 0$) and with equal flowrates ($q_1^* = q_2^*$) the concentration of precursor inside the reactor is half that flowing into it. This reflects the dilution that occurs due to the mixing of precursor and air inside the CSTR.

The stoichiometry of the two-step reaction, equations (15), (16), is used to eliminate either the fuel species ($\mathcal{B}^*$) or oxygen ($\mathcal{O}_2^*$) from the system.

$$\frac{\mathrm{d}}{\mathrm{d}t^*}\left[n\mathcal{F}^* + \mathcal{B}^* - \mathcal{O}_2^*\right] = n\left(\frac{\mathrm{d}\mathcal{F}^*}{\mathrm{d}t^*}\right) + \left(\frac{\mathrm{d}\mathcal{B}^*}{\mathrm{d}t^*}\right) - \left(\frac{\mathrm{d}\mathcal{O}_2^*}{\mathrm{d}t^*}\right) \tag{31}$$

$$= \left\{nq_1^*\alpha - 0.21q_2^*(1-\alpha)\right\} - \left(q_1^* + q_2^*\right)\left[n\mathcal{F}^* + \mathcal{B}^* - \mathcal{O}_2^*\right]. \tag{32}$$

Therefore, the expression $n\mathcal{F}^* + \mathcal{B}^* - \mathcal{O}_2^*$ approaches a steady-state exponentially in time. Thus under steady-state conditions, setting equation (32) to equal zero, we have the algebraic relationship

$$n\mathcal{F}^* + \mathcal{B}^* - \mathcal{O}_2^* = \frac{nq_1^*\alpha - 0.21q_2^*(1-\alpha)}{q_1^* + q_2^*}. \tag{33}$$

We use this equation to eliminate the fuel species from the model.

Under the assumption of adiabatic operation it is possible to eliminate either oxygen or the temperature variable from the model. This arises because the only route for heat-loss under these conditions also affects the species concentrations inside the reactor.

$$\frac{\mathrm{d}}{\mathrm{d}t^*}\left[\frac{Q_2^*\mathcal{P}^*}{T_0^*}\mathcal{O}_2^* + T^*\right] = \frac{Q_2^*\mathcal{P}^*}{T_0^*}\left(\frac{\mathrm{d}\mathcal{O}_2^*}{\mathrm{d}t^*}\right) + \left(\frac{\mathrm{d}T^*}{\mathrm{d}t^*}\right) \tag{34}$$

$$= \left\{0.21q_2^*(1-\alpha)\frac{Q_2^*\mathcal{P}^*}{T_0^*} + \left(q_1^* + q_2^*\right)T_0^*\right\} - \left(q_1^* + q_2^*\right)\left[\frac{Q_2^*\mathcal{P}^*}{T_0^*}\mathcal{O}_2^* + T^*\right]. \tag{35}$$

Therefore, the term $(Q_2^*\mathcal{P}^*/T_0^*)\mathcal{O}_2^* + T^*$ approaches a steady-state exponentially in time. Under steady-state conditions we have the algebraic relationship

$$\frac{Q_2^*\mathcal{P}^*}{T_0^*}\mathcal{O}_2^* + T^* = \frac{0.21q_2^*(1-\alpha)Q_2^*\mathcal{P}^*}{(q_1^* + q_2^*)T_0^*} + T_0^*. \tag{36}$$

Using equations (30), (36) the steady-state value for the fuel species is given by

$$\mathcal{B}^* = \frac{nq_1^*\alpha A_1^*}{(q_1^* + q_2^*)(q_1^* + q_2^* + A_1^*)} + \frac{T_0^*}{Q_2^*\mathcal{P}^*}\left(T_0^* - T^*\right). \tag{37}$$

Thus, under adiabatic operation the four-dimensional system given by equations (25)–(28) reduces to a one-dimensional system. Oscillatory behaviour for this scheme is, therefore, impossible under adiabatic operation. The multiplicity of the system is governed by the singularity function

$$\mathcal{G} = \left(q_1^* + q_2^*\right)\left(T_0^* - T^*\right) + \frac{Q_2^*A_2^*\mathcal{P}^{*^2}}{T_0^{*^2}}\exp\left[\frac{-E_2^*}{T^*}\right]\left\{\frac{nq_1^*\alpha A_1^*}{(q_1^* + q_2^*)(q_1^* + q_2^* + A_1^*)} + \frac{T_0^*}{Q_2^*\mathcal{P}^*}\left(T_0^* - T^*\right)\right\} \times \left\{\frac{0.21q_2^*\,(1-\alpha)}{q_1^* + q_2^*} + \frac{T_0^*}{Q_2^*\mathcal{P}^*}\left[T_0^* - T^*\right]\right\} \tag{38}$$

($\mathcal{G}$ is obtained by substituting equations (30), (33), (36) into equation (28) and investigating the system under steady state operating conditions).

Note that equation (38) can also be obtained by judicious addition and subtraction of the steady-state model, equations (25)–(28) with the time derivatives set to zero. However, this would not tell us anything about the existence or nonexistence of Hopf bifurcations. The advantage of obtaining the singularity function by the reduction of the model to one differential equation is that it shows that Hopf bifurcations cannot occur in the adiabatic reactor.

3.4. Numerics

The path following software program Auto 97 [49] was used to obtain steady-state and limit-point unfolding diagrams. In steady-state diagrams the standard representation is used: solid lines are stable steady states; and, dotted lines are unstable steady states.

Continuation methods require a known solution to begin calculations. Equations (25)–(28) have two "natural" starting places for continuation: no precursor species in the inflow ($\alpha = 0$) and no air in the inflow ($\alpha = 1$). The appropriate steady-state solutions are:

No fuel in the inflow ($\alpha = 0$):	No air in the inflow ($\alpha = 1$):	
$\mathcal{F}^* = 0,$	$\mathcal{F}^* = \dfrac{q_1^*}{q_1^* + q_2^* + A_1^*},$	(39)
$\mathcal{B}^* = 0,$	$\mathcal{B}^* = \dfrac{nA_1^*}{q_1^* + q_2^*} \cdot \dfrac{q_1^*}{q_1^* + q_2^* + A_1^*},$	(40)
$\mathcal{O}_2^* = \dfrac{0.21q_2^*}{q_1^* + q_2^*},$	$\mathcal{O}_2^* = 0,$	(41)
$T^* = \dfrac{(q_1^* + q_2^*)T_0^* + JT_a^*}{q_1^* + q_2^* + J},$	$T^* = \dfrac{(q_1^* + q_2^*)T_0^* + JT_a^*}{q_1^* + q_2^* + J}.$	(42)

4. Results

In sections 4.1–4.3 we investigate how the steady-state structure of our model varies as one of three experimentally controllable parameters is changed: the fuel fraction (α), the inflow temperature (T_0^*), or the total inflow pressure ($\mathcal{P}^*$). The feed rates of the fuel and air, q_1^* and q_2^*, respectively, are assumed fixed, although in principle they can also be manipulated experimentally. Finally, in section 4.4 we consider the effect of changing the precursor decay rate (A_1^*). Although this parameter is not experimentally controllable, it is usually taken as a primary bifurcation parameter in the single Sal'nikov model in order to establish the necessary conditions for which thermokinetic oscillations occur. We have already established that thermokinetic oscillations do not occur in an adiabatic CSTR. These investigations are carried out using the methodology outlined in section 1.2. Parameter values at which the double limit point variety occurs were not found. Thus, in the bifurcation diagrams, figures 2, 4 and 7, only the cusp and isola varieties are shown.

A feature of our nondimensionalisation scheme is that there is a one-to-one relationship between our dimensionless variables and their dimensional counterparts. Hence we write often, for example, "the inflow temperature", rather than "the dimensionless inflow temperature".

4.1. *Fuel fraction as the primary bifurcation parameter*

In this section the fuel fraction is regarded as the primary bifurcation parameter, with the inflow pressure and inflow temperature as the secondary continuation parameters. Recall from section 2.2 that when $n = 1$ the reaction mixture is said to be *fuel-lean* if $\alpha < 0.174$ and *fuel-rich* if $\alpha > 0.174$. The condition $\alpha = 0.174$ defines a stoichiometric mixture.

Figure 2 is a bifurcation diagram showing the cusp and isola locii in the inflow pressure-inflow temperature plane. These curves, parameterised by the fuel fraction,

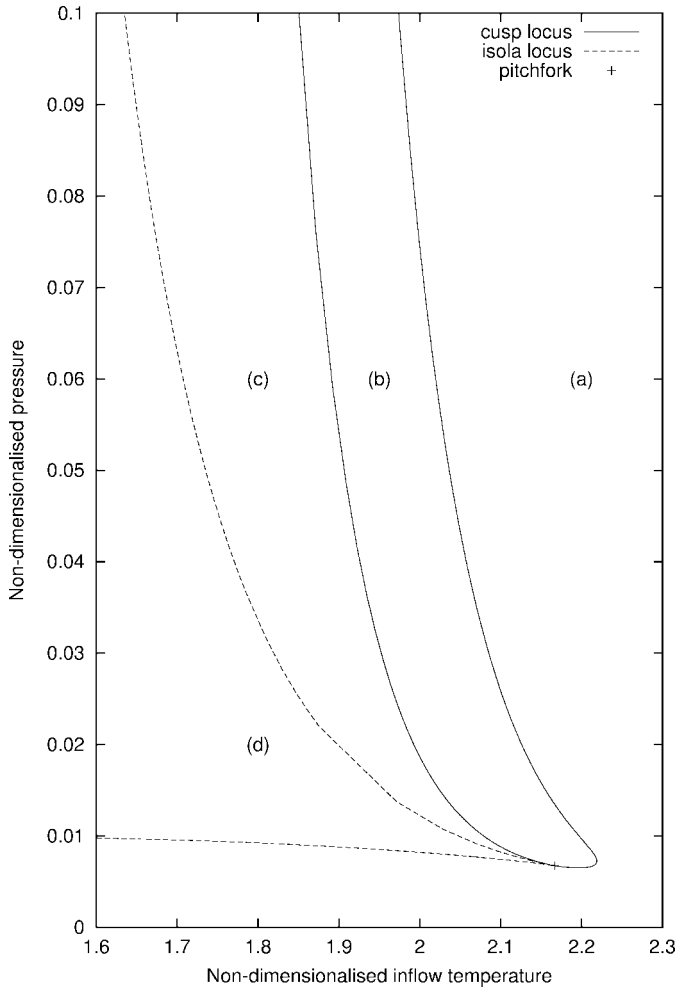

Figure 2. Bifurcation diagram in the inflow pressure-inflow temperature plane when fuel fraction is the distinguished bifurcation parameter. The marked regions correspond to: (a) unique steady-state; (b) single hysteresis loop (breaking wave); (c) double hysteresis loop (mushroom); and (d) isola. Typical steady-state diagrams from the four regions are shown in figure 3. Parameter value: dimensionless precursor decay rate, $A_1^* = 0.1$.

divide the plane into four regions. As explained in section 1.2 there are therefore four generic steady-state diagrams. The four regions coalesce at a point where the cusp and isola curves intersect tangentially. This point satisfies the equalities

$$\mathcal{G} = \mathcal{G}_{T^*} = \mathcal{G}_{T^*T^*} = \mathcal{G}_{\alpha} = 0 \tag{43}$$

and is therefore a pitchfork singularity [46]. Note that all four regions are found in a neighbourhood of this point. In the language of singularity theory the pitchfork is therefore an organising centre for this system.

The generic steady-state diagrams are illustrated in figure 3. Observe that in each diagram the maximum temperature occurs at $\alpha \approx 0.179$, a mixture that is on the fuel-

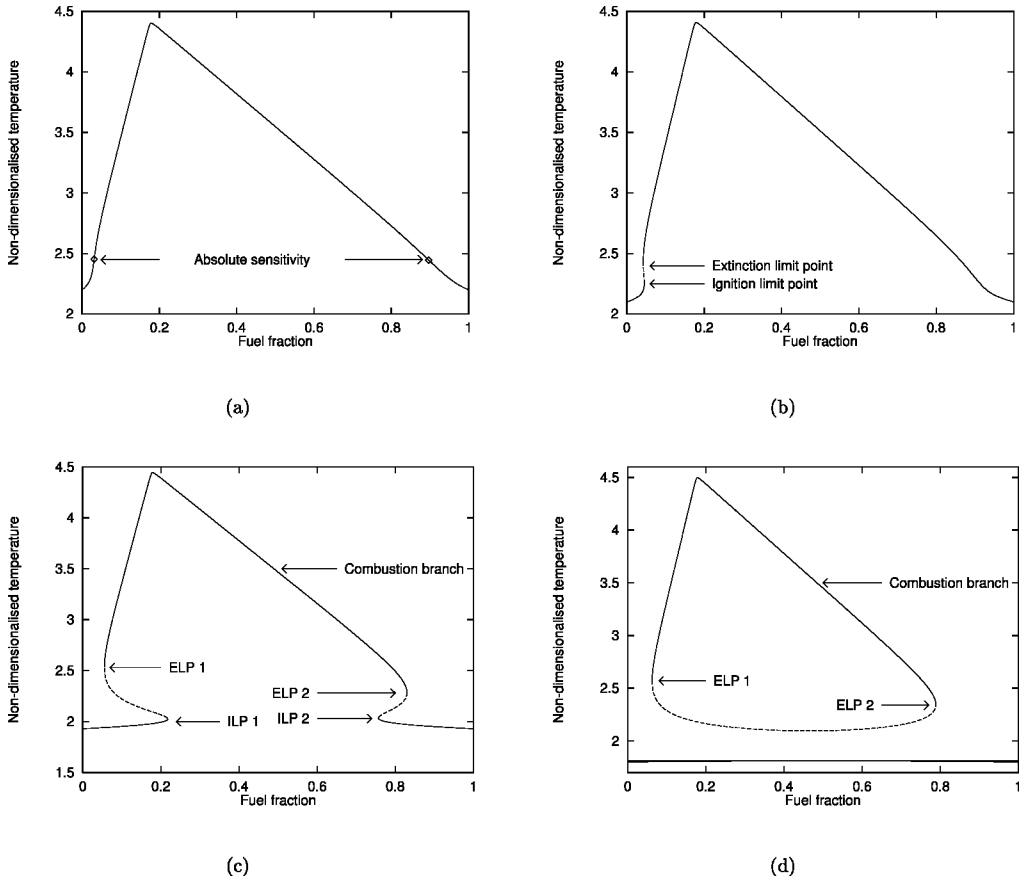

Figure 3. The four generic steady-state diagrams when fuel fraction is the primary bifurcation parameter: (a) unique, showing the points of absolute sensitivity discussed in section 5.2, (b) single hysteresis loop (breaking wave), (c) double hysteresis loop (mushroom), (d) isola. These figures correspond to a horizontal slice through figure 2 with $\mathcal{P}^* = 0.02$. The abbreviations ELP and ILP are extinction limit point and ignition limit point, respectively. Parameter values: dimensionless precursor decay rate, $A_1^* = 0.1$; dimensionless pressure, $\mathcal{P}^* = 0.02$; dimensionless inflow temperature, (a) $T_0^* = 2.2$, (b) $T_0^* = 2.1$, (c) $T_0^* = 1.93$, (d) $T_0^* = 1.8$.

rich side of stoichiometry. This is discussed further in section 5.1. Figure 3(a) shows a unique steady-state diagram. From a practical perspective there is a region on this figure in which the system is in a state of combustion, although there are no critical values of the fuel fraction at which abrupt changes in the temperature occur. Instead, ignition and extinction occur gradually. To see that a state of combustion exists observe that, for example, the maximum temperature on figure 3(a) is higher than that on some parts of the combustion branch on figures 3(c)–(d), even taking into account the higher inflow temperature for figure 3(a). Alternatively, if one starts in the vicinity of the maximum temperature on figure 3(d) and slowly increases the inflow temperature the sequence of steady-state diagrams shown in figures 3(d) to 3(a) are transversed. Eventually figure 3(a) is reached with only a small decrease in the steady-state temperature: combustion must have been maintained during this sequence. The concept of criticality for unique response curves is discussed in section 5.2.

Under the experimental conditions defined by figure 3(b) the response diagram contains a single hysteresis loop (such response diagrams are also known as breaking-waves). For fuel-lean mixtures ignition and extinction are defined by limit points at $\alpha = 4.479718 \cdot 10^{-2}$ and $\alpha = 4.216573 \cdot 10^{-2}$, respectively. At these values ignition (extinction) occurs suddenly as the fuel fraction is increased (decreased) from (towards) zero. There is a very small region over which the reactant composition defines a flammable mixture ($4.216573 \cdot 10^{-2} < \alpha < 4.479718 \cdot 10^{-2}$). For fuel-rich mixtures ignition (extinction) occurs gradually as the fuel fraction is decreased (increased) from (towards) one, similar to the situation in figure 3(a). The concept of criticality for fuel-rich mixtures in breaking-wave systems is discussed in section 5.2.

Figure 3(c) shows a double hysteresis loop (such response curves are frequently referred to as "mushrooms"). This system has two ignition limit points, at $\alpha = 0.202$ and $\alpha = 0.757$, and two extinction limit points, at $\alpha = 0.056$ and $\alpha = 0.830$. Thus, if either $\alpha < 0.056$ or $\alpha > 0.757$ the reaction mixture is nonflammable. If either $0.056 < \alpha < 0.202$ or $0.757 < \alpha < 0.830$ the mixture is flammable. Finally, if $0.202 < \alpha < 0.757$ autoignition occurs. When the response diagram is a mushroom, combustion of either very fuel-lean ($\alpha < 0.056$) or very fuel-rich ($\alpha > 0.830$) mixtures can be initiated abruptly by either increasing or decreasing the fuel fraction, respectively. This is in contrast to the single hysteresis loop response diagram, figure 3(b), where only very fuel-lean mixtures can be ignited abruptly.

A typical isola solution is shown in figure 3(d). This figure contains two disjoint solution branches: a low-valued no-ignition branch, on which the maximum temperature raise is approximately 3 K over the inflow temperature; and, an isola, which has stable and unstable branches. The isola has two extinction limit points at which combustion is extinguished, between these points the flame temperature varies smoothly with the fuel fraction. Flammability limits are identified with the extinction limit points: the lower flammability limit (fuel-lean flammability limit) is given as $\alpha = 0.062$ and the upper flammability limit (fuel-rich flammability limit) is given as $\alpha = 0.788$. Thus, in figure 3(d) a fuel-air mixture is flammable only if its composition is in the range $0.062 < \alpha < 0.788$. There are no ignition limit points on this figure. Consequently,

ignition cannot be initiated by changing the fuel fraction; an ignition source is required to ignite a flammable mixture.

The concept that there are limiting temperatures below which flames cannot propagate is often useful [50]. For example, it is possible to predict the effectiveness of a wide variety of fire-retardants based upon the premise that extinction occurs when sufficient heat has been removed by the additive to reduce the temperature to a critical value [14]. Critical "minimal flame temperatures" are identified in figures 3(c)–(d) as the steady-state temperature at the extinction limit points. In these figures the limiting fuel-lean flame temperature is higher than the limiting fuel-rich flame temperature. For the mushroom, these temperatures are $T^* = 2.535$ and $T^* = 2.285$, respectively, whereas for the isola they are $T^* = 2.572$ and $T^* = 2.344$. These values provide critical flame-temperatures for fuel–air mixtures. The temperature at the extinction limit when a retardant is present is not necessarily the same as that in the absence of the additive. In practice critical loadings can be calculated satisfactorily using a common limiting temperature [14].

4.2. Inflow temperature as the primary bifurcation parameter

In this section the inflow temperature is regarded as the primary bifurcation parameter, with the inflow pressure and fuel fraction as the secondary continuation parameters.

Figure 4 shows the cusp and isola locii in the inflow pressure–fuel fraction plane. These curves, parameterised by the inflow temperature, divide the plane into three regions and there is no organising centre. Figure 5 shows the three generic steady-state diagrams. In these subfigures the fuel fraction is fixed ($\alpha = 0.6$) and inflow pressure increased. All three subfigures contain two disjoint solution branches.

Figure 5(a) shows that in region (a) of figure 4 the response diagram contains a combustion branch and a unique equilibrium branch. The former contains one extinction limit point and no ignition limit points. The latter has no limit points and the steady-state temperature increases monotonically with increasing inflow temperature. Abrupt changes in the steady-state temperature (ignition) in this system cannot be initiated by smoothly changing the inflow temperature. The physical system defined by figure 5(a) is flammable for those inflow temperatures at which the combustion branch exists. However, from a practical perspective, this figure represents a fuel that is *not* flammable. The reason for this is that the combustion branch only exists at low temperatures ($T_0^* \leqslant 0.304$). The assumptions of the model would not apply at these temperatures, e.g., departure from ideal gas behaviour and even liquefaction of the reactants at sufficiently low inflow temperatures.

As the inflow pressure is increased, at a fixed fuel fraction of $\alpha = 0.6$, the cusp locus is crossed in figure 4. Figure 5(b) shows that the cusp point occurs on the monotonic branch, creating a steady-state diagram containing three limit points on two disjoint curves. There are now two combustion branches: combustion branch (1) which has an extinction limit point but no ignition limit point; and, combustion branch (2) which has

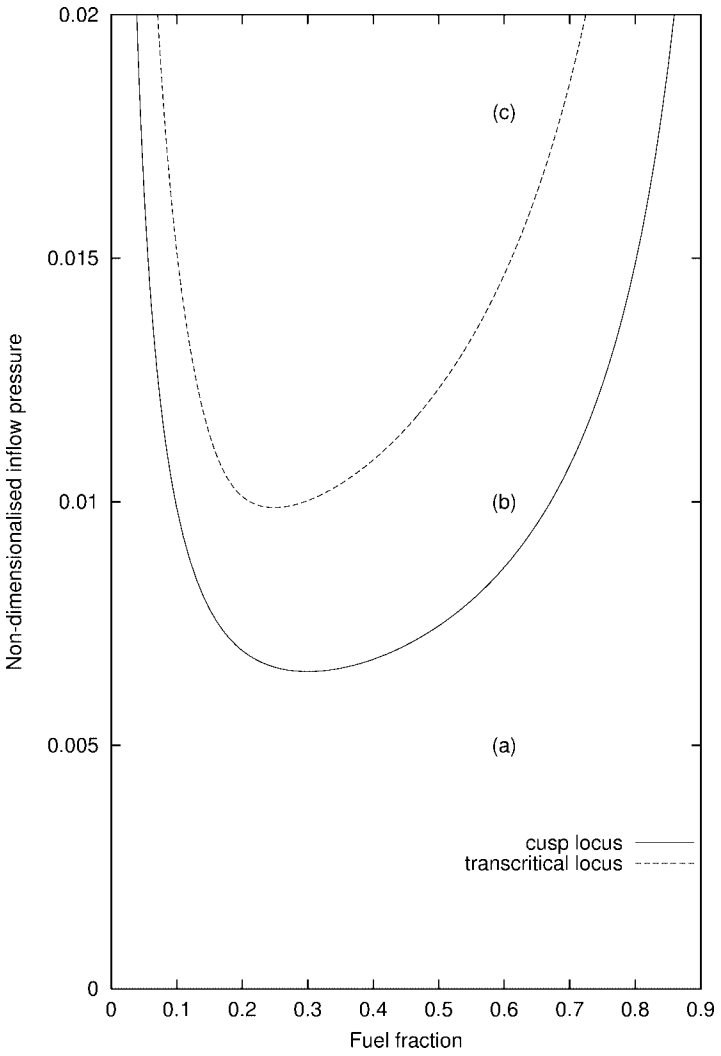

Figure 4. Bifurcation diagram in the inflow pressure-fuel fraction plane when inflow temperature is the distinguished bifurcation parameter. The marked regions correspond to: (a) unique solution branch + disjoint multi-valued branch; (b) breaking wave + disjoint multi-valued branch; and (c) multi-valued no-ignition branch + single-valued combustion branch. Typical steady-state diagrams from the three regions are shown in figure 5. Parameter value: dimensionless precursor decay rate, $A_1^* = 0.1$.

both an ignition and an extinction limit point. The inflow temperature at which the extinction limit point occurs on combustion branch (1) has increased and is now slightly higher than room temperature ($T_0^* = 1.032$). As a result some parts of this branch are now physically meaningful and would be experimentally accessible. Consequently, there are now two regions of the inflow temperature over which the reaction mixture is flammable: an upper region, between the inflow temperatures at which the second extinction limit point and the ignition limit point occur, and a lower region, bounded by

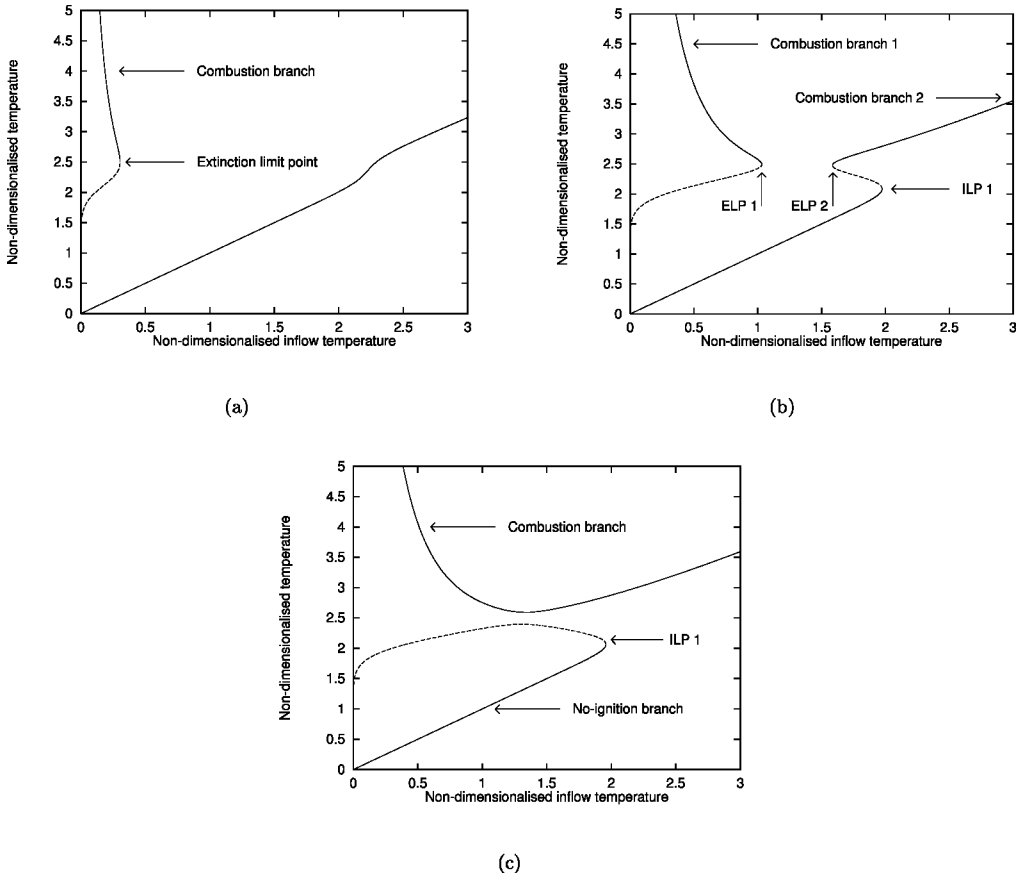

Figure 5. The three generic steady-state diagrams when inflow temperature is the primary bifurcation parameter: (a) unique solution + disjoint multi-valued branch, (b) breaking wave + disjoint multi-valued branch, (c) multi-valued no-ignition branch + single-valued combustion branch. These figures correspond to a vertical slice through figure 4 with value $\alpha = 0.6$. The abbreviations ELP and ILP are extinction limit point and ignition limit point, respectively. Parameter values: dimensionless precursor decay rate, $A_1^* = 0.1$; fuel fraction, $\alpha = 0.6$; dimensionless inflow pressure, (a) $\mathcal{P}^* = 6 \cdot 10^{-3}$, (b) $\mathcal{P}^* = 14 \cdot 10^{-3}$, (c) $\mathcal{P}^* = 15 \cdot 10^{-3}$.

the inflow temperature at the first extinction limit point and a lower value at which the assumptions of the model cease to hold.

As the inflow pressure is increased further the two extinction limit points in figure 5(b) approach each other. At criticality the two disjoint solution branches join together, splitting apart as the isola variety is crossed. As the steady-state curves on either side of the singularity contain disjoint solution branches the critical point is a transcritical singularity. Figure 5(c) has a no-ignition branch, containing one limit point, and a combustion branch, containing no limit points. The latter is defined for any inflow temperature. Consequently, once combustion is initiated it cannot be extinguished by

slowly varying the inflow temperature. This system defines a flammable mixture for values of the inflow temperature that lays between the inflow temperature at which the model breaks down and the ignition limit point. At sufficiently high values of the inflow temperature autoignition occurs. Again those parts of these two branches occurring at sufficiently low inflow temperatures – such as the origin – are not physically meaningful. Comparing figures 5(b), (c) observe that in effect the stable components of the two combustion branches have merged together to form one combustion branch whilst the two unstable components of the disjoint solution branches have formed the unstable component of the no-ignition branch.

Figure 6 shows the limit point unfolding diagram when the fuel fraction is fixed with $\alpha = 0.6$. In figure 6(a) the parameter values at which the transcritical and cusp singularities occur are identified. The range for inflow pressures over which the generic steady-state diagrams are found are marked. Although the generic steady-state diagrams contain two disjoint solution branches with different combinations of limit points on the branches the limit points are connected in the unfolding diagram. Figure 6(b) uses the unfolding diagram to identify the combustion phenomena occurring as a function of the inflow pressure and inflow temperature. The parameter plane is divided into three regions in which either ignition, slow reaction, or bistability is exhibited. The bistability region could be subdivided into two, depending upon if the assumptions of the model hold. Note that for sufficiently low pressure the steady-state diagram is given by figure 5(a) and the transition from "slow reaction" to ignition occurs gradually. Similarly at sufficiently high inflow temperature the steady-state diagram is similar to figure 8(a) and the transition is gradual.

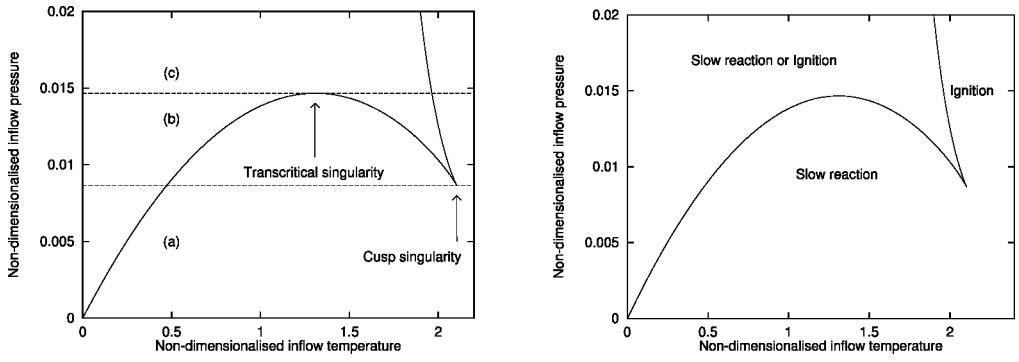

Figure 6. The limit point unfolding diagram in the inflow pressure-inflow temperature plane when the fuel fraction is $\alpha = 0.6$: (a) the domains of existence of the three generic steady-state diagrams in figure 5; (b) the pressure-inflow temperature ignition limit diagram. Parameter value: dimensionless precursor decay rate, $A_1^* = 0.1$.

4.3. *Inflow pressure as the primary bifurcation parameter*

In this section the inflow pressure is regarded as the primary bifurcation parameter, with the inflow temperature and the fuel fraction as the secondary continuation parameters.

Figure 7 shows the cusp locus in the inflow temperature–fuel fraction plane. In section 4.3.1 we show that the isola singularity does not occur when inflow pressure is the primary bifurcation parameter. The cusp locus, parameterised by the inflow pressure, divides the plane into two regions. Thus there are two generic steady-state diagrams. For a given value of the fuel fraction both regions are found in a neighbourhood of the corresponding cusp point. Thus the cusp singularity is an organising centre in this

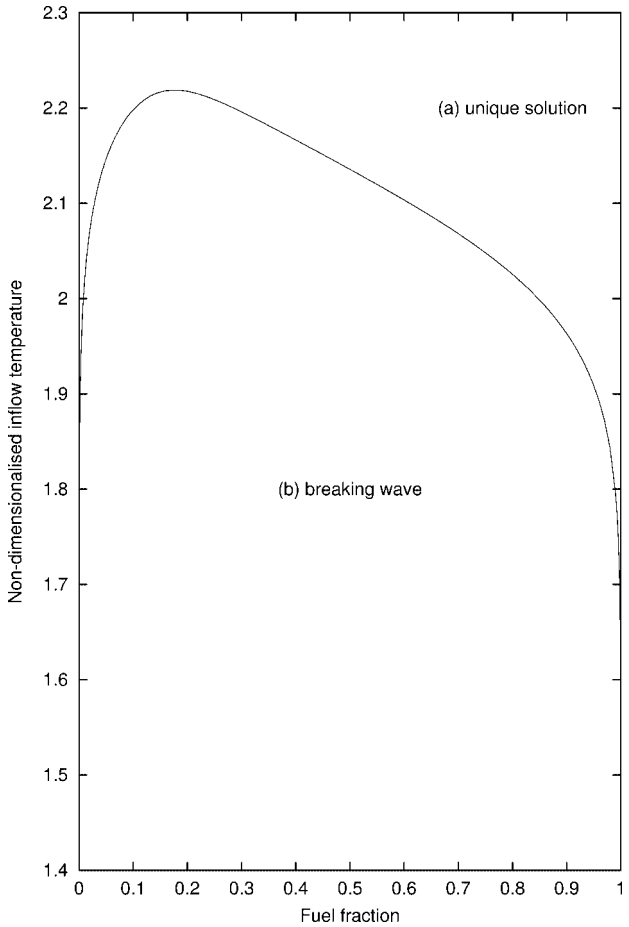

Figure 7. Bifurcation diagram in the inflow temperature–fuel fraction plane when inflow pressure is the distinguished bifurcation parameter. The marked regions correspond to: (a) unique steady-state; (b) single hysteresis loop (breaking wave). Typical steady-state diagrams from the two regions are shown in figure 8. Parameter value: dimensionless precursor decay rate, $A_1^* = 0.1$.

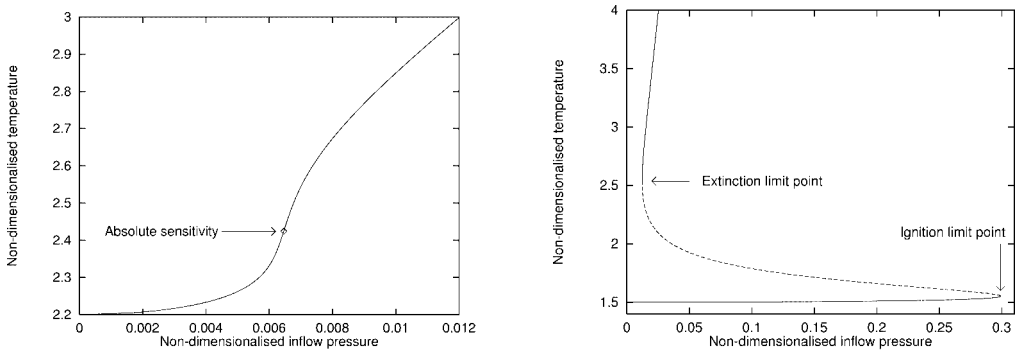

Figure 8. The two generic steady-state diagrams when inflow temperature is the primary bifurcation parameter: (a) unique solution, showing a point of absolute sensitivity, discussed in section 5.2, (b) breaking wave. These figures correspond to a vertical slice through figure 7 with value $\alpha = 0.50$. Parameter values: dimensionless precursor decay rate, $A_1^* = 0.1$; fuel fraction, $\alpha = 0.5$; dimensionless inflow temperature, (a) $T_0^* = 2.2$, (b) $T_0^* = 1.5$,

diagram.

In region (a) of figure 7 the response diagram is a unique steady-state, with the steady-state temperature increasing monotonically with increasing inflow pressure. This scenario is shown in figure 8(a). As the inflow temperature is decreased in figure 7 the cusp locus is eventually crossed. The steady-state diagram now contains an ignition limit point and an extinction limit point. This case is shown in figure 8(b). As can be seen from this figure the steady-state temperature increases rapidly with inflow pressure on the combustion branch.

From a practical perspective combustion occurs for the system represented by figure 8(a) at sufficiently high pressures. The increase in inflow pressure shown in this figure, from $\mathcal{P}^* = 0$ to $\mathcal{P}^* = 0.012$, has produced a dimensionless temperature increase of $T^* \approx 0.8$, approximately 240 K. This temperature increase, due to chemical reaction, will continue to grow as the pressure is increased and there will be a value of the inflow pressure at which it is not possible to study this system in a glass vessel. Criticality for unique solution structures is discussed in section 5.2.

4.3.1. Singularity theory when inflow pressure is the distinguished parameter

In this section we show that the equations $\mathcal{G} = 0$ and $\mathcal{G}_{\mathcal{P}^*} = 0$ cannot be satisfied simultaneously. Hence, when the inflow pressure is the experimentally manipulated parameter (distinguished parameter in singularity theory) isolas, transcritical bifurcations, pitchfork bifurcations, and various other higher-order singularities cannot occur.

It is convenient to rewrite equation (38) in the form

$$\mathcal{G} = Z\big(T_0^* - T^*\big) + Y\frac{\mathcal{P}^{*^2}}{T_0^{*^2}}\left[X + W\frac{T_0^*(T_0^* - T^*)}{\mathcal{P}^*}\right]\left[V + W\frac{T_0^*\left(T_0^* - T^*\right)}{\mathcal{P}^*}\right]. \qquad (44)$$

The functions V, W, X, Y and Z can be identified by inspection, whereupon it is seen that (recalling that $0 < \alpha < 1$)

$$V > 0, \quad W > 0, \quad X > 0, \quad Y = f(T) > 0, \quad Z > 0. \tag{45}$$

After some algebra it is found that the equation $\mathcal{G}_{\mathcal{P}^*} = 0$ has the solution

$$\mathcal{P}^* = -WT_0^*\left(T_0^* - T^*\right)\frac{(X+V)}{2XV}. \tag{46}$$

Substitution of this expression into equation (44) gives

$$0 = \left(T_0^* - T^*\right)\left\{Z - \frac{YW^2[X-V]^2}{4XV}\left(T_0^* - T^*\right)\right\}. \tag{47}$$

Thus, either

$$T^* = T_0^*, \tag{48}$$

or

$$T^* = T_0^* - 4\frac{XVZ}{W^2Y[X-V]^2}. \tag{49}$$

Equations (48), (49) show that if $\mathcal{G} = \mathcal{G}_{\mathcal{P}^*} = 0$, then the steady-state temperature is either equal to the inflow temperature, equation (48), or strictly less than the inflow temperature, equation (49). However, for $0 < \alpha < 1$ the steady-state temperature is always higher than the inflow temperature. Thus, we conclude that it is not possible for both $\mathcal{G}$ and $\mathcal{G}_{\mathcal{P}^*}$ to be simultaneously zero. As a result, the isola singularity, and related higher-order singularities, do not exist when inflow pressure is the distinguished parameter.

4.4. Precursor decay rate as the primary bifurcation parameter

In this section the precursor decay rate is regarded as the primary bifurcation parameter, with the inflow pressure, inflow temperature, and fuel fraction as the secondary continuation parameters. It is not possible to manipulate the preexponential factor of a chemical reaction experimentally. However, the Sal'nikov scheme represents an idealised chemical mechanism and it is usual to treat the decay rate as a distinguished parameter.

Differentiation of equation (38) gives

$$\mathcal{G}_{A_1^*} = \frac{Q_2^*A_2^*\mathcal{P}^{*^2}}{T_0^{*^2}}\exp\left[\frac{-E_2^*}{T^*}\right]\left\{\frac{0.21q_2^*(1-\alpha)}{q_1^*+q_2^*} + \frac{T_0^*}{Q_2^*\mathcal{P}^*}\left[T_0^* - T^*\right]\right\} \times \left\{\frac{nq_1^*\alpha}{(q_1^*+q_2^*+A_1^*)^2}\right\}. \tag{50}$$

The solution of $\mathcal{G}_{A_1^*} = 0$ is given by

$$T^* = T_0^* + \frac{Q_2^* \mathcal{P}}{T_0^*} \frac{0.21 q_2^* (1-\alpha)}{q_1^* + q_2^*}. \tag{51}$$

Substitution of equation (51) into equation (38) gives

$$\mathcal{G} = -0.21 q_2^* (1-\alpha) \frac{Q_2^* \mathcal{P}}{T_0^*} < 0 \quad \text{as } 0 < \alpha < 1. \tag{52}$$

It is, therefore, not possible to satisfy the equations $\mathcal{G} = 0$ and $\mathcal{G}_{A_1^*} = 0$ simultaneously. As a result, we again do not obtain the isola singularity and related higher-order singularities.

5. Discussion

5.1. The dependence of the maximum temperature upon fuel fraction

Our chemical mechanism consists of two consecutive reactions. In the first, the precursor species ($\mathcal{F}$) decomposes to produce a reductant ($\mathcal{B}$). In the second, one mole of $\mathcal{B}$ reacts with one mole of oxygen. Under ideal operating conditions the species $\mathcal{B}$ and $\mathcal{O}_2$ are completely consumed in the reactor. From this premise simple physical reasoning infers that as the fuel fraction is varied the maximum temperature inside the reactor should occur when the rate of production of species $\mathcal{B}$ inside the reactor is equal to the rate of inflow of oxygen. Under this condition the concentrations of fuel and oxygen are in their stoichiometric proportions, i.e., they are 1:1.

From equations (25), (27) the rate of production of fuel inside the reactor and the inflow of oxygen into the reactor are given by $n A_1^* \mathcal{F}^*$ and $0.21 q_2^* (1-\alpha)$, respectively. Under steady-state conditions the concentration of precursor species is given by equation (30). Thus, the maximum temperature should occur when the fuel fraction satisfies

$$n A_1^* \mathcal{F}^* = 0.21 q_2^* (1-\alpha), \tag{53}$$

$$\Rightarrow \quad n A_1^* \cdot \frac{q_1^* \alpha}{q_1^* + q_2^* + A_1^*} = 0.21 q_2^* (1-\alpha). \tag{54}$$

The critical value of the fuel fraction is, therefore,

$$\alpha = \frac{0.21 q_2^* (q_1^* + q_2^* + A_1^*)}{n A_1^* q_1^* + 0.21 q_2^* (q_1^* + q_2^* + A_1^*)}. \tag{55}$$

Equation (55) predicts that the maximum temperature only depends upon the inflow rates and the precursor decay rate. For the values used in figure 3 the maximum temperature is predicted to occur when $\alpha = 0.176$. This is a good approximation to the observed value ($\alpha \approx 0.179$).

Equation (55) is based upon simple physical reasoning. More accurately, the maximum temperature is found by viewing equation (38) as defining temperature as a function of fuel fraction and solving the system

$$\mathcal{G}\big(T^*(\alpha),\alpha\big)=0, \tag{56}$$

$$\mathcal{G}_\alpha\big(T^*(\alpha),\alpha\big)=0, \quad \text{subject to the condition } \frac{\mathrm{d}T^*}{\mathrm{d}\alpha}=0. \tag{57}$$

These equations do not have a simple solution giving the fuel fraction at which the maximum temperature occurs. Equation (57) is equivalent to solving $\mathcal{G}_\alpha = 0$. After some algebra the solution of the equation $\mathcal{G}_\alpha = 0$ is found to be

$$\alpha=\frac{1}{2}+\frac{(q_1^*+q_2^*)}{0.42nq_1^*q_2^*\mathcal{A}_1^*}\big[nq_1^*\mathcal{A}_1^*-0.21q_2^*\big(q_1^*+q_2^*+\mathcal{A}_1^*\big)\big]\frac{T_0^*(T_0^*-T^*)}{Q_2^*\mathcal{P}^*}. \tag{58}$$

Thus, we conclude that the critical value of the fuel fraction decreases as the precursor decay rate increases.

5.2. Criticality when the response diagram is single-valued

In figure 3(a) the response diagram has a unique solution for any value of the fuel fraction. As discussed in section 4.1 even though there are no limit points, there are values of the fuel fraction at which combustion occurs; a flame would be visible. Accordingly a definition of criticality for these systems is required. Similarly a demarcation of the slow-reaction/combustion boundary is required for figure 3(b) where combustion is initiated gradually as the fuel fraction is decreased from one and increased from zero respectively. (In figure 3(b) ignition is defined by a limit point bifurcation if the fuel fraction is increased from zero.) In these situations criticality can be defined using either absolute or normalised sensitivities. This concept was first applied to the interpretation of unique response curves in a CSTR by Chemburkar et al. [51].

As the fuel fraction is increased from zero in figure 3(a) "ignition" occurs somewhere in the range $0 < \alpha < \alpha_{\max}$, where $\alpha_{\max}$ is the fuel fraction at which the maximum temperature on the response diagram is found. A *pragmatic definition* for the slow-reaction/combustion transition in this region is to define criticality as the fuel fraction at which the modulus of the first derivative of temperature, as a function of the fuel fraction, has maximum value. At this point the temperature exhibits maximum absolute sensitivity to changes in the fuel fraction. As the fuel fraction is increased from $\alpha_{\max}$, "extinction" occurs somewhere in the region $\alpha_{\max} < \alpha < 1$ and an analogous identification of the "combustion/slow-reaction" boundary can be made. Congruous definitions are used when the fuel fraction is decreased from one. Hence, points of ignition and extinction when the fuel fraction is increased from zero are points of extinction and ignition when it is decreased from one. In figure 3(a) these points occur at $\alpha = 0.031$ and $\alpha = 0.900$.

Ignition and extinction can be defined in this way in the appropriate regions for the response diagrams shown in figures 3(b). Note that when limit points occur, e.g., as

the fuel fraction is increased from zero in figure 3(b), the maximum absolute sensitivity occurs at the appropriate limit point. This approach can also be used to define criticality for figure 5(a) (assuming that we are on the unique-branch) and figure 8(a). The point of absolute sensitivity in figure 8(a) occurs at $\mathcal{P}^* = 0.00646$.

5.3. Flammability limits

Although gaseous fuels such as methane and propane are commonly referred to as flammable, their mixtures with oxygen or air will only burn if the fuel concentration lies within sharply defined limits, known as the lower (fuel-lean) and upper (fuel-rich) flammability limits. Outside of these limits ignition and flame propagation cannot be initiated by the application of an external stimulus. Even if a reaction mixture lie within its flammability limits ignition requires the input of sufficient energy in a suitable form. The most widely used method to determine flammability limits is the US Bureau of Mines apparatus [52] which measures a mixture's propensity to propagate a flame up a tube. This apparatus is unsatisfactory for examining the effects that small quantities of gas-phase active fire-retardants have on flammability limits. Hirst et al. [53] introduced a new apparatus specifically for this purpose. In this method the criterion of flammability is defined in terms of the pressure rise inside a closed spherical vessel. Many other methods have been used in the literature to study inhibition and extinction.

The CSTR offers another approach to measure flammability limits. A system represented by an isola, e.g., figure 3(d), satisfies the standard concept of a flammable system: the flammability limits are identified with the extinction limit points and are consequently sharply defined; the system is bistable between the flammability limits; consequently, an ignition source is required to ignite a flammable mixture. The identification of flammability limits with extinction limit points on an isola as the composition of a reaction mixture is varied was first made by Spalding [54]. More generally, it is possible that stability is lost at a Hopf point on the isola curve [55]. Thus one or both of the flammability limits may correspond to a Hopf point. The effect of a fire-retardant can be investigated by determining how these limits change as the additive concentration is increased. Conceptually, one imagines that as the degree of retardancy increases the extinction limit points approach each other, eventually the isola is destroyed when they annihilate each other. This is the case for chemically inert additives in well-stirred closed-vessel experiments [56].

In figure 3(d) the flammability limits are $\alpha = 0.062$ and $\alpha = 0.788$. Two types of problems can be addressed. We can pick a particular value of the fuel fraction, e.g., $\alpha = 0.2$, and determine the additive concentration at which this mixture ceases to be flammable. Alternatively, we can determine a critical additive loading at which no air-fuel-additive mixture is flammable. The answer to the former is defined by the additive concentration at which an extinction limit point "passes through" the chosen value of the fuel fraction [56]. The answer to the latter is given by the additive concentration at which the isola is destroyed at the isola singularity [56]. In figure 2 this can be envisaged as crossing the boundary between regions (d) and (a).

The determination of a critical doping level at which a specified mixtures ceases to be flammable requires a large number of repetitive tests in both of the standard tests mentioned previously. One advantage of using a CSTR is that a state of combustion can be stabilised in the absence of the additive and then the additive concentration in the inflow slowly increased until combustion ceases. Thus one continuous experiment determines the limit.

From the perspective of flammability studies the existence of isolas is a desirable feature. In other applications, such as the operation of industrial reactors, they are undesirable: their presence leading to unexpected problems in the operation and start-up of reactors. As it is very easy to miss their presence in experimental studies it is helpful to be able construct figures similar to figure 2 showing operating conditions in which they occur and which are therefore to be avoided.

The isola is also found in the well studied FONI system as the flowrate is changed [1]. In this case the extinction limit points do not define flammability limits as the chemical system only contains one reactive component. They do, however, define operating conditions which should be avoided.

6. Conclusions

In this paper we have investigated the dynamics of a gaseous oxidation reaction in an adiabatic continuously stirred reactor. The chemical mechanism used is a modified single Sal'nikov scheme. The Sal'nikov mechanism has been extended so that the second step is a bimolecular reaction between a fuel species and oxygen. Ignition and extinction behaviour are now exhibited as the ratio of reactants flowing into the reactor is varied. The model contains a temperature equation and an equation each for the three chemical species. Under the assumption of adiabatic behaviour this system reduces to one equation. Consequently periodic solutions for this system are impossible under adiabatic conditions.

The main bifurcation parameters of interest in this study are the inflow pressure, the inflow temperature, and the fuel fraction. The steady-state structure of the model is investigated by applying the techniques of singularity theory. When inflow pressure is the distinguished parameter a pitchfork singularity is the organising centre. One of the steady-state diagrams generated by this point is the isola. This represents the standard understanding of flammability limits as the fuel fraction is varied. A simple theory, based upon physical reasoning, allows the fuel fraction at which the maximum temperature occurs to be accurately predicted.

When the inflow temperature is varied there are three steady-state structures. Both the hysteresis and the transcritical variety occur, an organising centre was not found. When the inflow pressure is varied it is shown that the isola singularity cannot occur. The organising centre in this case is the cusp singularity and there are two types of steady-state structure.

From the perspective of determining flammability the most important bifurcation parameter is the fuel fraction and the most important steady-state structure is the isola.

This figure defines flammability limits, outside of which fuel-air mixtures cannot sustain flames. The effectiveness of different classes of fire-retardants can be classified by investigating how the flammability limits change as the additive loading increases.

Acknowledgements

During this work MIN was supported by a grant from the the Australian Research Council. We thank an anonymous referee for bringing to our attention the paper by Simon et al. [48].

Appendix. Nomenclature

A superscript * refers to a dimensionless quantity, i.e., $\mathcal{P}^*$ is a dimensionless parameter whose dimensional counterpart is $\mathcal{P}$. The notation $\mathcal{V}(t=0)$ and $\mathcal{V}^*(0)$ refers to the initial value of the dimensional variable $\mathcal{V}$ at time $t=0$ and its dimensionless counterpart at time $t^*=0$.

A_1	Pre-exponential factor for the decomposition of the precursor species.	s^{-1}
A_1^*	$A_1^* = A_1 \cdot c_{p_\mathrm{g}} \rho_\mathrm{g} V_\mathrm{g} / \chi S$.	
A_2	Pre-exponential factor for the gas-phase oxidation reaction.	$\mathrm{m}^3 \cdot \mathrm{mol}^{-1} \cdot \mathrm{s}^{-1}$
A_2^*	$A_2^* = A_2 \cdot c_{p_\mathrm{g}} \rho_\mathrm{g} V_\mathrm{g} / \chi S \cdot \mathcal{P}_\mathrm{r}(RT_\mathrm{r})$.	
$\mathcal{B}$	The concentration of gaseous fuel $\mathcal{B}$ in the reactor.	$\mathrm{mol} \cdot \mathrm{m}^{-3}$
$\mathcal{B}^*$	$\mathcal{B}^* = \mathcal{B}/c_\mathrm{r}$.	
$\mathcal{B}^*(0)$	$\mathcal{B}^*(0) = \mathcal{B}_0/c_\mathrm{r}$.	
$\mathcal{C}$	The concentration of product species $\mathcal{C}$ in the reactor.	$\mathrm{mol} \cdot \mathrm{m}^{-3}$
E_2	Activation energy for the gas-phase oxidation reaction.	$\mathrm{J} \cdot \mathrm{mol}^{-1}$
E_2^*	$E_2^* = E_2/(RT_\mathrm{r})$.	
$\mathcal{F}$	The concentration of the precursor species in the reactor.	$\mathrm{mol} \cdot \mathrm{m}^{-3}$
$\mathcal{F}^*$	$\mathcal{F}^* = \mathcal{F}/c_\mathrm{r}$.	
$\mathcal{F}^*(0)$	$\mathcal{F}^*(0) = \mathcal{F}(0)/c_\mathrm{r}$.	
$\mathcal{F}_0$	The concentration of the precursor species in the reactant inflow tube: $\mathcal{F}_0 = \mathcal{P}_\mathrm{f}/RT_0$.	$\mathrm{mol} \cdot \mathrm{m}^{-3}$
$\mathcal{F}_0^*$	$\mathcal{F}_0^* = \mathcal{F}_0/c_\mathrm{r} = \mathcal{P}_\mathrm{f}/(RT_0) \cdot RT_0/\mathcal{P}_0 = \mathcal{P}_\mathrm{f}/\mathcal{P}_0 = \alpha$.	
J	A constant. $J=0$ corresponds to adiabatic operation.	
$\mathcal{O}_2$	The concentration of oxygen in the reactor.	$\mathrm{mol} \cdot \mathrm{m}^{-3}$
$\mathcal{O}_2^*$	$\mathcal{O}_2^* = \mathcal{O}_2/c_\mathrm{r}$.	
$\mathcal{O}_2^*(0)$	$\mathcal{O}_2^*(0) = \mathcal{O}_2(0)/c_\mathrm{r}$.	
$\mathcal{O}_{2,0}$	The concentration of oxygen in the inflow: $\mathcal{O}_{2,0} = 0.21\mathcal{P}_\mathrm{air}/(RT_0) = 0.21(\mathcal{P}_0 - \mathcal{P}_\mathrm{f})/(RT_0)$.	$\mathrm{mol} \cdot \mathrm{m}^{-3}$
$\mathcal{O}_{2,0}^*$	$\mathcal{O}_{2,0}^* = \mathcal{O}_{2,0}/c_\mathrm{r} = 0.21(1-\alpha)$.	
$\mathcal{P}^*$	Dimensionless total pressure: $\mathcal{P}^* = \mathcal{P}_0/\mathcal{P}_\mathrm{r}$.	

$\mathcal{P}_r$	A reference pressure.	$J \cdot m^{-3}$
$\mathcal{P}_0$	The total pressure of the inflow reactants: $\mathcal{P}_0 = \mathcal{P}_{air} + \mathcal{P}_f$.	$J \cdot m^{-3}$
Q_2	Exothermicity of the oxidation reaction.	$J \cdot mol^{-1}$
Q_2^*	$Q_2^* = Q_2 \cdot \mathcal{P}_r/(RT_r) \cdot 1/(c_{p_g}\rho_g T_r)$.	
R	Ideal gas constant.	$J \cdot K^{-1} \cdot mol^{-1}$
S	The internal surface area of the reactor.	m^2
T	The temperature inside the reactor.	K
T^*	$T^* = T/T_r$.	
$T(0)$	The temperature inside the reactor at time $t = 0$.	K
$T^*(0)$	$T^*(0) = T(0)/T_r$.	
T_a	The temperature of the reactor walls.	K
T_a^*	$T_a^* = T_a/T_r$.	
T_r	The reference temperature scale.	K
T_0	The temperature of the inflow.	K
T_0^*	$T_0^* = T_0/T_r$.	
V_g	Volume of the reactor.	m^3
c_{p_g}	Heat capacity of the reaction mixture.	$J \cdot K^{-1} \cdot kg^{-1}$
c_r	Reference concentration: maximum concentration of an ideal gas assembled at a pressure $\mathcal{P}_0$ and temperature T_0, $c_r = \mathcal{P}_0/(RT_0)$.	$mol \cdot m^{-3}$
n	The number of moles of gaseous fuel ($\mathcal{B}$) produced by the decomposition of 1 mole of reactant $\mathcal{A}$.	
q_1	The flowrate through the reactant tube into the reactor.	$m^3 \cdot s^{-1}$
q_1^*	$q_1^* = q_1 \cdot c_{p_g}\rho_g/\chi S$.	
q_2	The flowrate through the oxygen tube into the reactor.	$m^3 \cdot s^{-1}$
q_2^*	$q_2^* = q_2 \cdot c_{p_g}\rho_g/\chi S$.	
t	Time.	s
t^*	$t^* = t \cdot \chi S/c_{p_g}\rho_g V_g$.	
α	The fraction of fuel (by partial pressure) in the inflow: $\alpha = \mathcal{P}_f/\mathcal{P}_0$.	
ρ_g	Density of the reaction mixture.	$kg \cdot m^{-3}$
χ	Heat transfer coefficient between the reaction mixture and the reactor walls.	$J \cdot s^{-1} \cdot m^{-2} \cdot K^{-1}$

Unless otherwise specified we take the following typical parameter values: $A_2 = 10^9$ $m^3 \cdot mol^{-1} \cdot s^{-1}$, $E_2 = 114.737478 \cdot 10^3$ $J \cdot mol^{-1}$, $Q_2 = 500 \cdot 10^3$ $J \cdot mol^{-1}$, $S = 7.6766 \cdot 10^{-2}$ m^2, $T_0 = 600$ K, $V = 2 \cdot 10^{-3}$ m^3, $c_{p_g} = 638.4814$ $J \cdot kg^{-1} \cdot K^{-1}$, $n = 1$, $q_1 = V_g/16$ $m^3 \cdot s^{-1}$, $q_2 = V_g/16$ $m^3 \cdot s^{-1}$, $\rho_g = 0.038$ $kg \cdot m^{-3}$, $\chi = 39.0798$ $J \cdot s^{-1} \cdot m^{-2} \cdot K^{-1}$.

The appropriate values for physical constants are: $R = 8.31441$ $J \cdot K \cdot mol^{-1}$.

We take $P_r = 1.01325 \cdot 10^5$ $J \cdot m^{-3}$, $T_r = 298$ K.

Typically mean residence times $t_{res} = V_g/(q_1 + q_2)$ are of the order of seconds and are variable over about a three- to sixfold range. The value taken for the flowrates in this

paper gives a typical residence time for a molecule in the reactor of 8 s. This fits into the range of values commonly used.

References

[1] L.F. Razon and R.A. Schmitz, Multiplicities and instabilities in chemically reacting systems – a review, Chem. Engrg. Sci. 42(5) (1987) 1005–1047.
[2] V. Caprio, A. Insola and R. Barbella, Preflame processes in the ozone activated oxidation of methlycyclopentane, in: *Combustion Institute European Symposium 1973*, ed. F.J. Weinberg (Academic Press, New York, 1973) pp. 99–104.
[3] V. Caprio, A. Insola and P.G. Lignola, Isobutane cool flames investigation in a continuous stirred tank reactor, in: *Sixteenth International Symposium on Combustion* (The Combustion Institute, 1976) pp. 1155–1163.
[4] P.G. Felton, B.F. Gray and N. Shank, Low temperature oxidation in a stirred flow reactor – II. Acetaldehyde, Combustion and Flame 27 (1976) 363–376.
[5] B.F. Gray and P.G. Felton, Low-temperature oxidation in a stirred-flow reactor – I. Propane, Combustion and Flame 23 (1974) 295–304.
[6] B.F. Gray, P.G. Felton and N. Shank, A theoretical and experimental study of the low temperature oxidation of acetaldehyde, in: *2nd European Symposium on Combustion* (The Combustion Institute, 1975) p. 103.
[7] T. Faravelli, P. Gaffuri, E. Ranzi and J.F. Griffiths, Detailed thermokinetic modelling of alkane autoignition as a tool for the optimization of performance of internal combustion engines, Fuel 77(3) (1998) 147–155.
[8] J.F. Griffiths, Thermokinetic oscillations in homogeneous gas-phase oxidations, in: *Oscillations and Travelling Waves in Chemical Systems*, eds. R.J. Field and M. Burger (Wiley, New York, 1985) pp. 529–564.
[9] P. Gray and S.K. Scott, Experimental systems 2: Gas-phase reactions, in: *Chemical Oscillations and Instabilities: Nonlinear Chemical Kinetics*, International Series of Monographs on Chemistry, Vol. 21 (Clarendon Press, 1990) chapter 15.
[10] J.F. Griffiths and S.K. Scott, Thermokinetic interactions: Fundamentals of spontaneous ignition and cool flames, Progr. Energy Combust. Sci. 13 (1987) 161–197.
[11] I.Y. Sal'nikov, A thermokinetic model of homogeneous periodic reactions, Doklady Akademii Nauk SSSR 60(3) (1948) 405–408 (in Russian).
[12] I.Y. Salnikov, Contribution to the theory of the periodic homogenous chemical reactions II. A thermokinetic self-excited oscillating model, Zhurnal Fizicheskoi Khimii 23 (1949) 258–272 (in Russian).
[13] L.P. Russo and B.W. Bequette, Impact of process design on the multiplicity behaviour of a jacketed exothermic CSTR, AIChe J. 41(1) (1995) 135–147.
[14] C.T. Ewing, J.T. Hughes and H.W. Carhart, The extinction of hydrocarbon flames based on the heat-absorption processes which occur in them, Fire and Materials 8(3) (1984) 148–155.
[15] B.F. Gray, Unified theory of explosions, cool flames and two-stage igntions, Part 1, Trans. Faraday Soc. 65 (1969) 1603–1613.
[16] C.H. Yang and B.F. Gray, Unified theory of explosions, cool flames and two stage ignitions, part 2, Trans. Faraday Soc. 65 (1969) 1614–1622.
[17] B.F. Gray and M.J. Roberts, Analysis of chemical kinetic systems over the entire parameter space I. The Sal'nikov thermokinetic oscillator, Proc. Roy. Soc. London Ser. A 416 (1988) 391–402.
[18] B.F. Gray and M.J. Roberts, An asymptotic analysis of the Sal'nikov thermokinetic oscillator, Proc. Roy. Soc. London Ser. A 416 (1988) 425–441.
[19] P. Gray, Instabilities and oscillations in chemical reactions in closed and open systems, Proc. Roy. Soc. London Ser. A 415 (1988) 1–34.

[20] P. Gray, S.R. Kay and S.K. Scott, Oscillations of an exothermic reaction in a closed system I. Approximate (exponential) represenation of an Arrhenius temperature-dependence, Proc. Roy. Soc. London Ser. A 416 (1988) 321–341.
[21] S.R. Kay and S.K. Scott, Oscillations of simple exothermic reactions in a closed system II. Exact Arrhenius kinetics, Proc. Roy. Soc. London Ser. A 416 (1988) 343–359.
[22] J.G. Burnell, J.G. Graham-Eagle, B.F. Gray and G.C. Wake, Determination of critical ambient temperature for thermal ignition, IMA J. Appl. Math. 42 (1989) 147–154.
[23] B.F. Gray, J.H. Merkin and G.C. Wake, Disjoint bifurcation diagrams in combustion systems, Math. Comput. Modelling 15(11) (1991) 25–33.
[24] B.F. Gray and G.C. Wake, On the determination of critical ambient temperatures and critial initial temperatures for thermal ignition, Combustion and Flame 71 (1988) 101–104.
[25] L.K. Forbes, Limit-cycle behaviour in a model chemical reaction: the Sal'nikov thermokinetic oscillator, Proc. Roy. Soc. London Ser. A 430 (1990) 641–651.
[26] H.N. Moreira and W. Yuquan, Sufficient conditions for the Sal'nikov equation to have at least two limit cycles, J. Math. Chem. 15 (1994) 63–72.
[27] L.K. Forbes and B.F. Gray, Forced oscillations in an exothermic chemical reaction, Dynamics and Stability of Systems 9(3) (1994) 253–269.
[28] E.J. Delgado R., Complex dynamics in a simple exothermic reaction model, Latin American Applied Research 24 (1994) 109–115.
[29] E.J. Delgado, Chaos in a spherical chemical reactor, Boletin Sociedad Chilena Quimica 40 (1995) 17–24.
[30] E.J. Delgado, A.F. Münster and F.W. Schneider, Chaos control and tracking of periodic states in a forced thermokinetic oscillator model, Berichte der Bunsen-Gesellschaft Physical Chemistry 99(8) (1995) 1049–1056.
[31] E.J. Delgado R., A thermal engine driven by a thermokinetic oscillator, J. Phys. Chem. 100(26) (1996) 11144–11147.
[32] L.K. Forbes, M.R. Myerscough and B.F. Gray, On the presence of limit-cycles in a model exothermic chemical reaction: Sal'nikov's oscillator with two temperature-dependent reaction rates, Proc. Roy. Soc. London Ser. A 435 (1991) 591–604.
[33] B.F. Gray and L.K. Forbes, Analysis of chemical kinetic systems over the entire parameter space IV. The Sal'nikov oscillator with two temperature-dependent reaction rates, Proc. Roy. Soc. London Ser. A 444 (1994) 621–642.
[34] M.J. Sexton and L.K. Forbes, An exothermic chemical reaction with linear feedback control, Dynamics and Stability of Systems 11(3) (1996) 219–238.
[35] U.S. Herges and E.H. Twizell, A finite-difference method for the numerical solution of the Sal'nikov thermokinetic oscillator problem, Proc. Roy. Soc. London Ser. A 449 (1995) 255–271.
[36] D.P. Coppersthwaite, J.F. Griffiths and B.F. Gray, Oscillations in the $H_2 + Cl_2$ reaction: experimental measurements and numerical simulation, J. Chem. Phys. 95(18) (1991) 6961–6967.
[37] P. Gray and J. Griffiths, Thermokinetic combustion oscillations as an alternative to thermal explosion, Combustion and Flame 78 (1989) 87–98.
[38] J.F. Griffiths, S.R. Kay and S.K. Scott, Oscillatory combustion in closed vessels: Theoretical foundations and their experimental verification, in: *Twenty-Second International Symposium on Combustion* (The Combustion Institute, 1988) pp. 1597–1607.
[39] H.S. Sidhu, M.J. Sexton, M.I. Nelson, G.N. Mercer and R.O. Weber, A simple combustion process in a semibatch reactor, in: *EMAC 2000 Proceedings*, eds. R.L. May, G.F. Fitz-Gerald and I.H. Grundy (The Institution of Engineers, Australia, 2000) pp. 251–254.
[40] M. Golubitsky and D. Schaeffer, *Singularities and Groups in Bifurcation Theory*, Applied Mathematical Sciences 51, Vol. 1, 1st ed. (Springer, New York, 1985).
[41] M. Golubitsky and D. Schaeffer, A theory for imperfect bifurcation theory via singularity theory, Comm. Pure Appl. Math. 32 (1979) 21–98.

[42] V. Balakotaiah and D. Luss, Analysis of the multiplicity patterns of a CSTR, Chem. Engrg. Commun. 13 (1981) 111–132.
[43] V. Balakotaiah and D. Luss, Analysis of the multiplicity patterns of a CSTR, Chem. Engrg. Commun. 19 (1982) 185–189.
[44] V. Balakotaiah and D. Luss, Structure of the steady-state solutions of lumped-parameter chemically reacting systems, Chem. Engrg. Sci. 37(11) (1982) 1611–1623.
[45] V. Balakotaiah and D. Luss, Global analysis of the multiplicity features of multi-reaction lumped-parameter systems, Chem. Engrg. Sci. 39(5) (1984) 865–881.
[46] M. Golubitsky and D. Schaeffer, The classification theorem, in: *Singularities and Groups in Bifurcation Theory*, Vol. 1, 1st ed. (Springer, New York, 1985) chapter IV, paragraph 2 pp. 196–202.
[47] V. Balakotaiah, Steady-state multiplicity features of open chemically reacting systems, in: *Reacting Flows: Combustion and Chemical Reactors, Part II*, ed. G.S.S. Ludford, Lectures in Applied Mathematics, Vol. 24 (American Mathematical Society, Providence, RI, 1986) pp. 129–161.
[48] P.L. Simon, H. Farkas and M. Wittman, Constructing global bifurcation diagrams by the parametric representation method, J. Comput. Appl. Math. 108 (1999) 157–176.
[49] E.J. Doedel, T.F. Fairgrieve, B. Sandstede, A.R. Champneys, Y.A. Kuznetsov and X. Wang, AUTO 97: Continuation and bifurcation software for Ordinary Differential Equations (with HomCont) (March 1998). Available by anonymous ftp from ftp.cs.concordia.ca/pub/doedel/auto.
[50] D. Drysdale, *An Introduction to Fire Dynamics*, 2nd ed. (Wiley, New York, 1999).
[51] R.M. Chemburkar, M. Morbidelli and A. Varma, Parametric sensitivity of a CSTR, Chem. Engrg. Sci. 41(6) (1986) 1647–1654.
[52] H.F. Coward and G.W. Jones, Limits of flammability of gases and vapours, in: *Bulletin* (United States Bureau of Mines, 1952) p. 503.
[53] R. Hirst, N. Savage and K. Booth, Measurement of inerting concentrations, Fire Safety J. 4 (1981/82) 147–168.
[54] D.B. Spalding, A theory of inflammability limits and flame-quenching, Proc. Roy. Soc. London Ser. A 240 (1957) 83–100.
[55] H.S. Sidhu, M.I. Nelson, G.N. Mercer and R.O. Weber, Dynamical analysis of an elementary $X+Y \rightarrow P$ reaction in a continuously stirred tank reactor, J. Math. Chem. 28(4) (2000) 353–375.
[56] M.I. Nelson, Flammability limits in batch reactor: a Semenov model, submitted.